ACS APPLIED MATERIALS & INTERFACES

Research Article

www.acsami.org

TiO_2 Nanoparticles-Functionalized N-Doped Graphene with Superior Interfacial Contact and Enhanced Charge Separation for Photocatalytic Hydrogen Generation

Zhigang Mou,[†,‡] Yijie Wu,[†] Jianhua Sun,[‡] Ping Yang,*[,†] Yukou Du,[†] and Cheng Lu*[,§]

[†]College of Chemistry, Chemical Engineering and Materials Science, Soochow University, Suzhou 215123, China

[‡]School of Chemistry and Environmental Engineering, Jiangsu University of Technology, Changzhou 213001, China

[§]Department of Chemistry, University of Toronto, Toronto M5S 3H6, Canada

Supporting Information

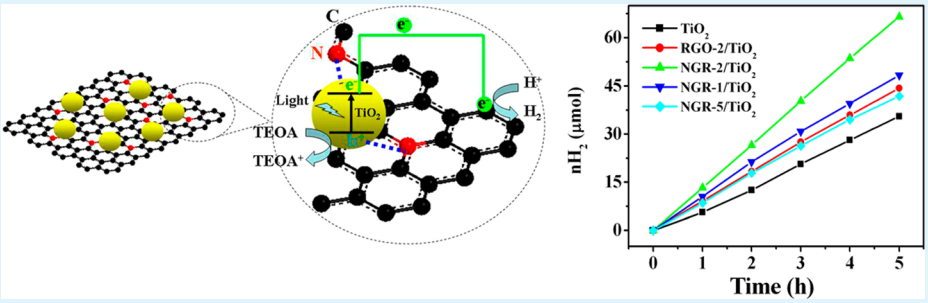

ABSTRACT: Titanium dioxide (TiO_2) nanoparticles-functionalized N-doped graphene (NGR) composites (NGR/TiO_2) were prepared through solvothermal treatment approach using exfoliated NGR and tetrabutyl titanate as the staring materials. The composites were characterized by transmission electron microscopy, X-ray diffraction, X-ray photoelectron spectroscopy, UV−vis diffuse reflectance spectra, photoelectrochemical, and electrochemical measurements. Nitrogen doping provides favorable nucleation and anchor sites for TiO_2 nanocrystals formation on NGR sheets, helping to form an intimate interfacial contact between NGR and TiO_2 nanoparticles. Moreover, NGR has higher electrical conductivity than the reduced graphene oxide (RGO) due to the recovery of the sp^2 graphite network and decrease of defects, resulting in more effective charge transfer and charge separation in the NGR/TiO_2 composite. NGR/TiO_2 nanocomposite demonstrated a higher photocatalytic activity for hydrogen production as compared to its counterpart, TiO_2-functionalized RGO composite (RGO/TiO_2). This work provides new insights to design new more efficient graphene-based nanocomposite photocatalysts for solar energy conversion.

KEYWORDS: *N-doped graphene, TiO_2, nanocomposite photocatalyst, platinum, hydrogen generation*

1. INTRODUCTION

Graphene has shown great promise for applications in electronics,[1] biosensor,[2] catalysis,[3−5] energy storage and conversion[6,7] due to its extraordinary electronic, thermal, and mechanical properties.[8,9] It has been widely reported that graphene incorporated semiconductor photocatalysts show enhanced photocatalytic performance for hydrogen generation because graphene performed as an excellent supporting matrix for semiconductor as well as an electron acceptor/transporter in the catalysts,[10−13] and thus efficiently reduced the recombination of the photogenerated electron−hole pairs and led to high photoconversion efficiency.[4,14,15]

TiO_2 as a photostable, inexpensive, and nontoxic photocatalyst has been widely explored in the field of solar energy conversion devices.[16] Incorporation of graphene or the reduced graphene oxide (RGO) with TiO_2 improved the photocatalytic activity for H_2 evolution.[17−21] However, the defects and some oxygen-containing groups remaining on RGO sheets not only reduce the electrical conductivity but also can become the recombination center of the photoexcited charges. Besides, the poor interfacial interaction between graphene and TiO_2 is another crucial factor that affects photocatalytic activity.[22] To solve these problems, Liang et al.[23] used the solvent-exfoliated graphene as a graphene precursor to minimize the defects of graphene/TiO_2 composite and to enhance the photocatalytic performance for CO_2 reduction. Xu's group[24] used polyvinylpyrrolidone-modified solvent-exfoliated graphene to prepare graphene/TiO_2 composite for both decreasing defects of graphene and improving the interfacial contact between graphene and TiO_2.

Both theoretical and experimental studies have revealed that nitrogen doping provides an effective approach to tailor the electronic property and chemical reactivity of the graphene.[25,26] N-Doped graphene (NGR) can anchor the metal nanoparticles

Received: May 23, 2014
Accepted: July 31, 2014
Published: July 31, 2014

for use in catalytic reactions[27] or directly participate in catalytic reactions.[28] Some methods, including the arc discharge,[29] chemical vapor deposition,[30] NH_3 plasma treatment,[31] the solvothermal reaction,[32] and thermal annealing graphene oxide (GO) with NH_3,[33] have been developed to produce NGR. We have also recently reported a simple approach to produce NGR by the thermal solid-state reaction of GO and urea.[34] In this thermal solid-state reaction process, N-doping is accompanied by the reduction of GO. NGR demonstrated great enhancement of electronic conductivity due to the recovery of the sp^2 graphene network and the decrease of defects within the plane associated with nitrogen incorporation.[35] As a semiconductor supporter, NGR has shown higher photocatalytic performance for hydrogen generation than the undoped one. For example, Jia et al.[36] demonstrated NGR/CdS photocatalyst displayed higher photocatalytic activity than RGO/CdS and GO/CdS due to the enhanced electron transportation from CdS to NGR.[37] Pei et al.[38] reported that the photocatalytic efficiency of NGR/N-TiO_2 composite under ultraviolet irradiation was improved greatly as compared to that of commercial P25. In addition, NGR/MoS_2[39] and NGR/ZnSe[40] photocatalysts also exhibited remarkably enhanced photocatalytic activities. These results suggest NGR as a cocatalyst of semiconductor is a more promising candidate to improve photocatalytic performance. However, it has rarely been reported the interfacial interaction between NGR and semiconductor nanoparticles relative to the nitrogen doping and its effects on the photoinduced charge transfer and photocatalytic performance.

In this work, we use solvent-exfoliated NGR as a supporting matrix to prepare NGR/TiO_2 nanocomposite for photocatalytic hydrogen generation from water. NGR has better electrical conductivity than RGO; moreover, our experimental results suggest nitrogen atoms in graphene can serve as favorable nucleation and anchor sites for TiO_2 nanocrystals to realize an intimate interfacial contact between NGR and TiO_2 nanoparticles. The photocatalytic activity test indicated that high photocatalytic activities for hydrogen generation were achieved by NGR/TiO_2 rather than pure TiO_2 and the RGO/TiO_2 composite. Furthermore, NGR enhances the photocatalytic stability of platinum nanoparticles-modified NGR/TiO_2 composites.

2. EXPERIMENTAL SECTION

2.1. Sample Preparation. GO was synthesized from purified natural graphite flakes using a modified Hummers method,[41] and then was annealed with urea at 700 °C to obtain NGR with ~10 at. % nitrogen content according to our previous method.[34,42] NGR/TiO_2 photocatalysts were synthesized in two steps using NGR and tetrabutyl titanate (TBOT) as the starting materials. Take the preparation of NGR/TiO_2 nanocomposite with 1 wt % NGR loading, for example: First, 7 mg of NGR was dispersed into 20 mL of water with sonication for 1 day, resulting in a metastable gray dispersion. The dispersion was then allowed to settle overnight. The precipitates at the bottom were removed (about 3.7 mg), and 80 mL of ethanol was then added to the remaining dispersion. The mixture was then sonicated for an additional 1 h, resulting in a stable suspension that did not show precipitation for weeks. Next, 426 mg of TBOT mixed with 10 mL of ethanol was added dropwise to 30 mL of the above NGR suspension (0.033 mg mL^{-1}) under magnetic stirring. After being stirred for 2 h, the mixture was transferred into a stainless steel autoclave with a 100 mL Teflon liner and kept at 180 °C for 10 h. The resulting precipitate was collected, washed thoroughly with distilled water followed by ethanol, and then dried at 80 °C to get the final NGR/TiO_2 nanocomposite. Similarly, a series of NGR/TiO_2 nanocomposites with different mass ratios of NGR were prepared. The samples prepared by this procedure were denoted as NGR-x/TiO_2, where x refers to the mass ratio of NGR relative to the mass of TiO_2. For comparison, RGO/TiO_2 nanocomposites were prepared following the same procedure as above except that GO suspension was used instead of NGR suspension. By this solvothermal treatment, GO can be converted to RGO using ethanol as reducing agent.[43] The pure RGO was prepared by the above solvothermal method using GO as a precursor. The pure TiO_2 was also prepared according to the same procedure described above for the preparation of NGR/TiO_2, in which NGR suspension was absent.

The platinum nanoparticles-modified NGR/TiO_2 nanocomposites were prepared by the photodeposition method according to the literature.[44] 332 μL of H_2PtCl_6 aqueous solution (7.723 mmol L^{-1}) and 50 mg of NGR/TiO_2 were added into 50 mL of alcohol aqueous solution (containing 20 vol % alcohol) in a quartz flask to load 1.0 wt % Pt on the surface of NGR/TiO_2, and then irradiated by a GY-10 xenon lamp (150 W) at room temperature for 2 h with continuous stirring under argon atmosphere. The sample was obtained by centrifugation and dried at 60 °C overnight. The platinized RGO/TiO_2 and TiO_2 catalysts were also prepared by using the same method.

2.2. Characterization. Transmission electron microscopy (TEM) images were recorded on a Hitachi S-4800 system. X-ray diffraction (XRD) patterns were measured on a Philips diffractometer with Ni-filtered Cu Kα radiation. UV−vis diffuse reflectance spectra were obtained on a Hitachi UV-3010 spectrophotometer using $BaSO_4$ as a reference. X-ray photoelectron spectroscopy (XPS) measurements were taken by an AXIS Ultra DLD system (Kratos Analytical Inc.) using monochromatic Al Kα radiation. The binding energies were calibrated with 284.6 eV for C 1s. Electrical conductivities of the NGR and RGO samples were ca. 40.0 and 3.5 S cm^{-1}, respectively, which were measured by four-point probe method under ambient conditions.

2.3. Photoelectrochemical and Electrochemical Measurements. All photoelectrochemical and electrochemical measurements were performed on a CHI 660B potentiostat/galvanostat electrochemical analyzer in a typical three-electrode configuration system using the prepared samples as the working electrodes, a saturated calomel as a reference electrode, and a platinum wire as a counter electrode. The electrolyte was 0.5 M Na_2SO_4 aqueous solution. The working electrodes were prepared as follows: the sample powder was thoroughly mixed with ethanol (100 mg mL^{-1}), and the obtained paste was applied evenly onto 1 cm^2 conducting indium tin oxide (ITO) glass substrate, resulting in a ca. 10 μm thick film. The transient photocurrents were recorded when the working electrode was irradiated with a 150 W xenon lamp. The electrochemical impedance spectroscopy (EIS) was measured under the perturbation signal of 5 mV over the frequency range from 1 to 100 MHz. The scan rate was 50 mV s^{-1} for the cyclic voltammograms (CV) measurement.

2.4. Photocatalytic Reaction. The photocatalytic reaction was carried out in a 50 mL quartz flask equipped with a flat optical entry window. A specified amount of the sample was added to 50 mL aqueous solution of triethanolamine (TEOA) (10 vol %). The pH of the solution was adjusted to the required value by the addition of 1 M hydrochloric acid solution. The system was deaerated by bubbling argon into the solution for 30 min before the reaction. The solution was stirred continuously and irradiated by a 150 W GY-10 xenon lamp (from ultraviolet to near-infrared full-spectrum emission) at 298 K and atmospheric pressure. The distance between the window of the flask and light source was 20 cm. The focused incident light intensity on the flask was ca. 80 mW cm^{-2}. The gases produced were analyzed through the online gas chromatograph (GC102AT) equipped with a TCD detector.

The apparent quantum yield (AQY) was measured under the same photocatalytic reaction condition except for the incident light through a band-pass filter (365 nm). The H_2 yields of 1 h photoreaction were measured. The photon flux of the monochromatic light was determined using a UV-A radiometer (made in the photoelectric instrument factory of Beijing Normal University, China). AQY values at 365 nm were calculated according to the following equation:

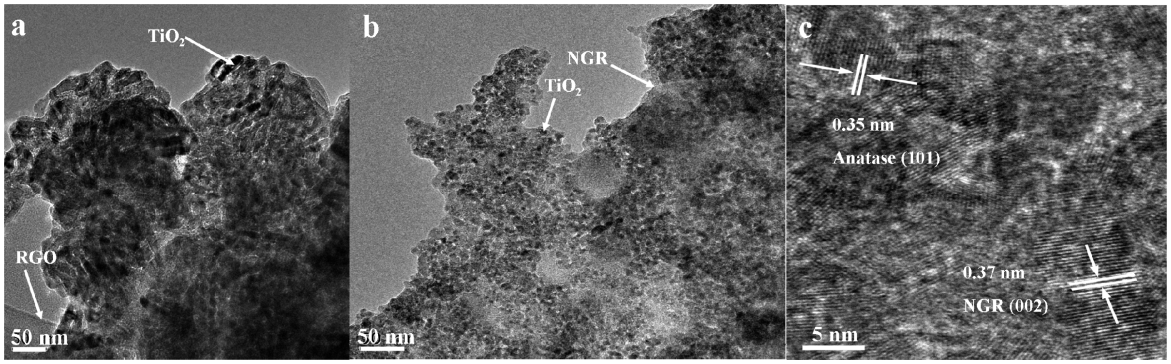

Figure 1. TEM images of (a) RGO-2/TiO_2 and (b) NGR-2/TiO_2; HRTEM image of (c) NGR-2/TiO_2.

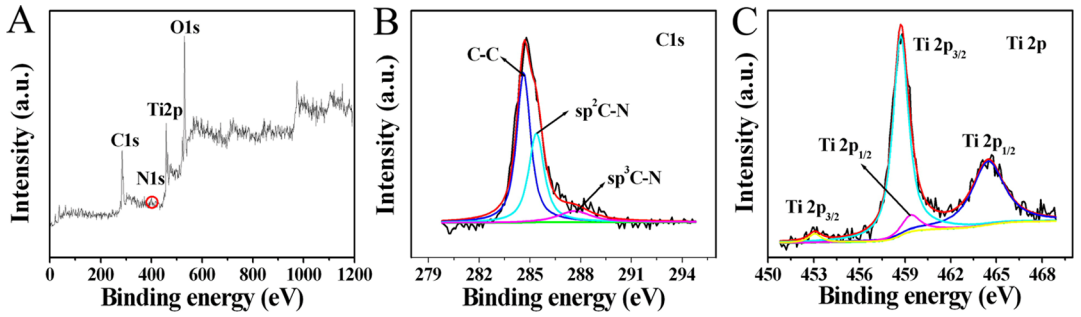

Figure 2. XPS survey spectrum of (A) NGR-2/TiO_2; HR-XPS spectra for (B) the C 1s region and (C) the Ti 2p region of NGR-2/TiO_2.

$$\text{AQY (\%)} = \frac{\text{number of reacted electrons}}{\text{number of incident photons}} \times 100$$

$$= \frac{\text{number of evolved } H_2 \text{ molecules} \times 2}{\text{number of incident photons}} \times 100$$

3. RESULTS AND DISCUSSION

3.1. Morphology and Structure Characterization of Samples. Figure 1 shows the TEM images of the as-prepared samples. For RGO-2/TiO_2 composite, the TEM image (Figure 1a) reveals that the average diameter of TiO_2 nanoparticles is ca. 20 nm, while for the sample NGR-2/TiO_2, TiO_2 nanoparticles with an average diameter of 8 nm are well distributed to the surface of NGR sheets (Figure 1b). HRTEM image of NGR-2/TiO_2 (Figure 1c) indicates that the TiO_2 nanoparticles and NGR are highly crystalline with a lattice spacing of ca. 0.35 and 0.37 nm, respectively, which correspond to the (101) plane of anatase TiO_2 and the (002) plane of graphene, respectively. Nitrogen-containing groups in graphene may serve as favorable nucleation and anchor sites for TiO_2 nanocrystals. The smaller size of TiO_2 nanoparticles in the NGR-2/TiO_2 system might be due to the stronger coupling between TiO_2 and N-doped sites on the NGR.[45] A similar phenomenon was also observed in the Co_3O_4/NGR system where the Co_3O_4 nanocrystal has a smaller size on NGR than that on RGO.[46] The strong coupling between TiO_2 and NGR contributes to the interfacial contact of the two moieties.

The XRD patterns of NGR/TiO_2 samples display distinct diffraction peaks (2θ) at 25.3°, 37.9°, 48.1°, 54.5°, 62.5°, 69.7°, and 75.2° (Figure S1 in the Supporting Information), which correspond to the (101), (004), (200), (105), (204), (220), and (215) crystalline planes of anatase TiO_2 (JCPDS card: 73-1764), respectively. Average crystallite size as estimated by the Scherrer equation from the fwhm of anatase TiO_2 (200) peak is ca. 8 ± 2 nm, which is consistent with the TEM observation. No diffraction peaks attributed to the NGR species were observed mainly due to the low amount and relatively low diffraction intensity of graphene.[11]

The XPS survey spectrum of NGR-2/TiO_2 confirms the elemental compositions. The XPS peaks at 284.6, 399.1, 460.5, and 530.1 eV (Figure 2A) can be assigned to the binding energies of C 1s, N 1s, Ti 2p, and O 1s, respectively.[47] HR-XPS for the C 1s region are resolved and can be fitted into three peaks centered at 284.6, 285.4, and 287.7 eV (Figure 2B), corresponding to the C−C, sp^2C−N, and sp^3C−N species, respectively.[30] There are no significant changes as compared to our previous report in NGR sample,[34] suggesting covalent C−N bonds are stable during the preparation process of the composite. For the HR-XPS of Ti 2p region (Figure 2C), the two prominent peaks centered at 458.7 and 464.5 eV correspond to Ti $2p_{3/2}$ and Ti $2p_{1/2}$ of TiO_2, respectively.[48] The two weak resolved peaks centered at 453.1 and 459.4 eV also relate to Ti $2p_{3/2}$ and Ti $2p_{1/2}$ at different chemical bonding environments, indicating the interaction between the Ti and nitrogen. The decrease of binding energies of two weak Ti $2p_{3/2}$ and Ti $2p_{1/2}$ peaks can be ascribed to the partial reduction of Ti^{4+} by the formation of N−Ti−O bonding because nitrogen has lower electronegativity than oxygen.[49,50] The interaction between the Ti and carbon can be excluded because no obvious changes of the C 1s peak in NGR/TiO_2 are observed.

Figure 3 shows the Raman spectra of TiO_2, RGO-2/TiO_2, and NGR-2/TiO_2 composite. For TiO_2, the main characteristic peak of anatase TiO_2 located at 150 cm^{-1} is attributed to the main E_g anatase vibration mode. The vibration peaks at 404 cm^{-1} (B_{1g}), 519 cm^{-1} (A_{1g}), and 644 cm^{-1} (E_g) indicate the anatase TiO_2 crystallites.[51] This observation is in well agreement with the XRD results. For RGO-2/TiO_2 and NGR-2/TiO_2 composite, the main E_g vibration mode shows

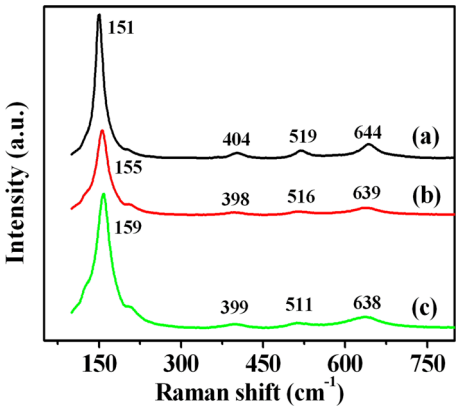

Figure 3. Raman spectra of (a) pure TiO_2, (b) RGO-2/TiO_2, and (c) NGR-2/TiO_2 composite.

an obvious blue-shift as compared to pure TiO_2, while the Raman peaks at 404, 519, and 644 cm^{-1} are shifted to lower wavenumbers. Although the blue-shift for the E_g mode of the composite is partially related to the quantum size confinement effect,[52] all of the shifts of the Raman peaks indicate the strong interactions between TiO_2 and RGO/NGR.[53,54] The larger Raman shifts in NGR/TiO_2 indicate a stronger interaction between TiO_2 and NGR than that for RGO.

3.2. Optical Properties and Charge Migration Study of Samples. The UV–vis diffuse reflectance spectra (Figure S2 in the Supporting Information) show that the absorption edge of NGR supported TiO_2 is red-shifted as compared to that of TiO_2, indicating NGR in the nanocomposite narrows the band gap of TiO_2 semiconductor.[14,55]

The CV curves of the samples are presented in Figure 4. NGR/TiO_2 electrode displays a large current density at

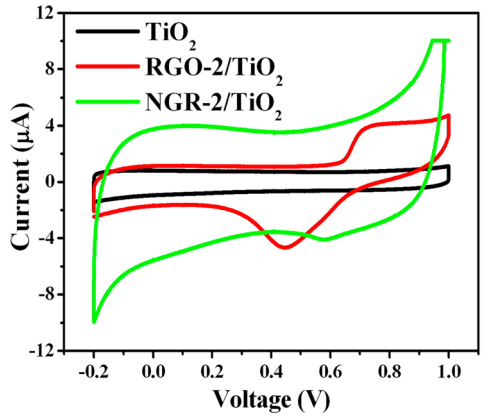

Figure 4. Cyclic voltammogram curves for the electrodes covered with TiO_2, RGO-2/TiO_2, and NGR-2/TiO_2 films in 0.5 M Na_2SO_4 electrolyte.

different potentials as compared to that of pure TiO_2 and RGO/TiO_2, demonstrating an obvious electron transfer rate enhancement due to the high conductivity of NGR. In addition, the curve of RGO/TiO_2 shows a clear cathodic peak around 0.45 V and an anodic peak around 0.7 V. The large peak-to-peak separation (ΔE_p) indicates poor redox reversibility of RGO/TiO_2.[43] For the NGR/TiO_2, the redox peaks are almost negligible, which indicate good charge propagation at the electrode surface.[56]

The transient photocurrents at different TiO_2 working electrodes were measured to better understand the charge transfer in the nanocomposite. For all samples, the rise and fall of the photocurrents responded rapidly with the on and off of the light-irradiation (Figure 5A). The photocurrent rapidly decreased to zero at dark state, and quickly increased to and was maintained at maximum value once the light was switched on. The photocurrent density of NGR/TiO_2 under light irradiation was about 7.0 $\mu A\ cm^{-2}$, whereas those of the TiO_2 and RGO/TiO_2 were about 1.5 and 4.5 $\mu A\ cm^{-2}$, respectively. The higher photocurrent in graphene composites suggests a higher charge transfer rate, which facilitates the efficient electron–hole separation and retard charge recombination.[24,57] Because the electrical conductivity of NGR (~40 S cm^{-1}) is much higher than that of RGO achieved by this solvothermal reduction (3.5 S cm^{-1}), thus NGR/TiO_2 demonstrates the higher carrier transfer rate and photocurrent density. In addition, introduction of nitrogen to the graphene network increases the electronic density of states near the Fermi level,[58] and thus facilitates interfacial electron transfer from TiO_2 to NGR sheets. To further investigate the effect of RGO and NGR on the charge transport efficiency, EIS presented as Nyquist plots were performed for the working electrodes of TiO_2, RGO/TiO_2, and NGR/TiO_2. As shown in Figure 5B, both RGO/TiO_2 and NGR/TiO_2 composite showed smaller curvatures of impedance arcs in the plot as compared to their pure TiO_2 counterpart, indicating the introduction of NGR/RGO in the nanocomposites improved the conductivity of the film.[59,60] Furthermore, the smaller arc of NGR/TiO_2 as compared to RGO/TiO_2 indicates a more rapid charge transport rate in the NGR/TiO_2 composite.

3.3. Photocatalytic Study. Photocatalytic activities for H_2 production on various samples were evaluated under 150 W xenon lamp irradiation. Figure 6 shows the effect of the concentration of NGR-2/TiO_2 on the amount of hydrogen evolved under experimental conditions. With the increase of NGR-2/TiO_2 amount, the amount of H_2 generation first increased. The amount of hydrogen evolved was 68.6 μmol in 5 h UV–vis irradiation when the concentration of the photocatalyst reached 0.6 mg mL^{-1}. Further increase of the NGR-2/TiO_2 amount led to a decrease of the amount of evolved H_2. The excess of photocatalyst in the photocatalytic system may block the penetration of the incident light in the suspension, and thus decrease the amount of H_2 evolution.[61]

The pH value of the reaction system also affects hydrogen evolution under experimental conditions (Figure S3 in the Supporting Information). When the pH values vary from 10.8 (without pH adjustment) to 6, the amount of hydrogen evolution decreased to a minimum at pH 6, indicating that basic solution was favorable to hydrogen evolution in our case. The result is similar to the results reported in the literature.[62] The decrease of hydrogen amount was related to the decreased ability to donate electrons of TEOA at low pH values.[63]

Figure 7A illustrates a typical time course of H_2 production over pure TiO_2, NGR/TiO_2, and RGO/TiO_2 from a TEOA aqueous solution (pH 10.8) under 150 W Xe-lamp illumination. In general, the NGR/TiO_2-based photocatalysts exhibit much higher activities. The content of NGR in the composite has an important influence on catalytic activity. The amount of evolved hydrogen increased with the increase of amount of NGR incorporated in the composite. The photocatalyst with optimized composition containing ca. 2 wt % NGR (NGR-2/TiO_2) shows the highest photocatalytic

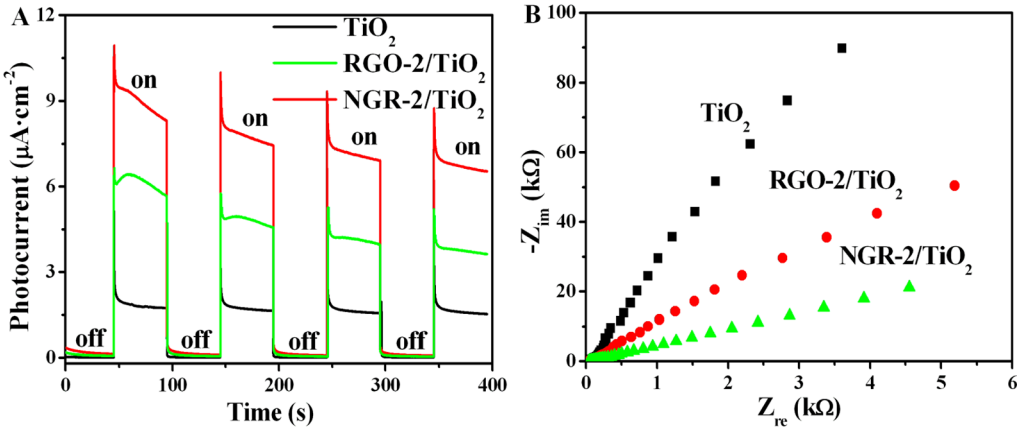

Figure 5. (A) The transient photocurrent responses of TiO_2, RGO-2/TiO_2, and NGR-2/TiO_2 to light irradiation recorded at 0.5 V. The illumination was interrupted every 50 s. (B) Nyquist plots of electrochemical impedance spectra for the electrodes covered with TiO_2, RGO-2/TiO_2, and NGR-2/TiO_2 films in 0.5 M Na_2SO_4 electrolyte.

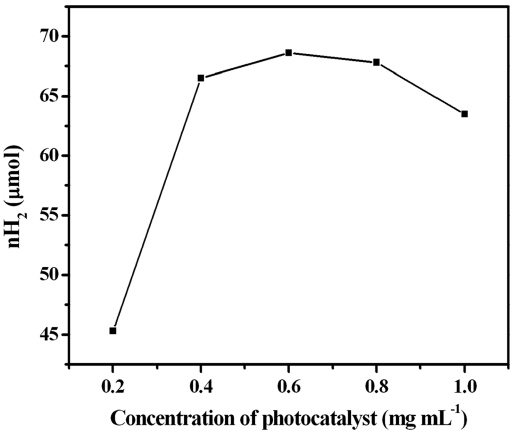

Figure 6. Effect of the concentration of NGR-2/TiO_2 on the amount of hydrogen evolved. Experimental conditions: 50 mL of aqueous solution of TEOA (10 vol %); pH 10.8; reaction time, 5 h; light source, a 150 W xenon lamp.

activity. The average rate of H_2 evolution of NGR-2/TiO_2 was 13.3 μmol h^{-1}, and the corresponding AQY was 3.5% at 365 nm, which was about double that of TiO_2 (7.1 μmol h^{-1}). However, excess NGR in the composite decreases photocatalytic activity because the high NGR incorporation in the nanocomposite may produce a filter effect or block the active sites of TiO_2.[64−66] Comparing the photocatalytic activity of NGR-2/TiO_2 with that of RGO-2/TiO_2, it is easy to find that NGR-2/TiO_2 has higher photocatalytic activity than RGO-2/TiO_2 (8.9 μmol h^{-1}). The photocatalytic results demonstrate that NGR as a cocatalyst of semiconductor is superior to RGO in the photocatalytic H_2 production in our case. To further confirm this, we compared the efficacy of the NGR-2/TiO_2 system with the other reported RGO-based TiO_2 systems in terms of material preparation, particle size, sacrificial electron donors used, and the rate of hydrogen production, as shown in Table 1. The TiO_2 particle size in NGR-2/TiO_2 composite is smaller than that in the other reported RGO/TiO_2 system using a similar preparation method. The average rate of H_2 evolution of NGR-2/TiO_2 is also higher than those of RGO/TiO_2 composites. It should be noted that no hydrogen evolution was observed in NGR/TiO_2 and RGO/TiO_2 composites under visible light irradiation (λ > 420 nm) in our case, indicating that the hydrogen produced from the NGR/TiO_2 and RGO/TiO_2 composites was mainly from UV-light contribution. The results also indicate the direct photoexcitation substance is TiO_2 rather than NGR/RGO. Figure 7B illustrated the photocatalytic hydrogen production mechanism of NGR/TiO_2 composite from TEOA aqueous solution. NGR as well as RGO in the nanocomposite not only serve as a scaffold to anchor semiconductor nanoparticles but also act as a charge acceptor due to its two-dimensional π-conjugation structure.[67,68] RGO sheet has irreversible defects such as large vacancies and disrupted conjugation sites in the plane resulting from harsh oxidization of GO;[33,69] besides, RGO prepared by the reduction of GO is usually not

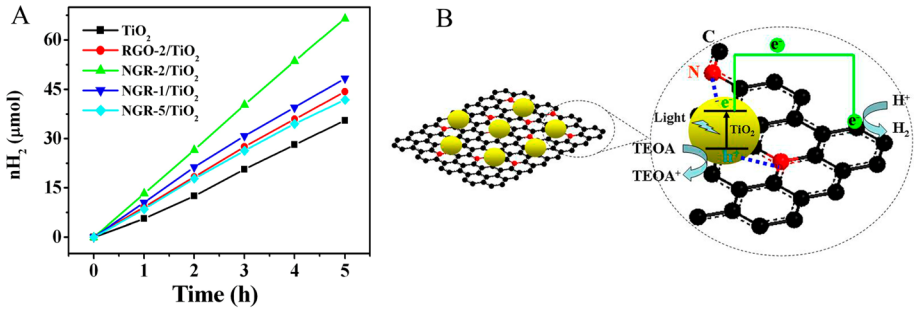

Figure 7. (A) The time course of hydrogen production from a 50 mL aqueous solution containing 10 vol % TEOA aqueous solution with different photocatalysts (20 mg, 0.4 mg mL^{-1}). pH 10.8; light source, a 150 W Xe lamp. (B) Schematic illustration for the strong coupling between TiO_2 and N atoms in NGR sheets and enhanced photoinduced charge transfer and photocatalytic hydrogen generation.

Table 1. Comparison of Hydrogen Generation over Various Graphene-Based TiO_2 Photocatalysts

catalyst	GC (wt %)[a]	TP[b]	PM[c]	PS (nm)[d]	illumination	SR[e]	R (μmol h^{-1})[f]	ref
RGO/TiO_2	2.0	$TiCl_4$	hydrothermal	15	500 W Xe lamp	Na_2S + Na_2SO_3	5.4	20
RGO/TiO_2	5.0	TBOT	sol−gel	10−15	500 W Xe lamp	Na_2S + Na_2SO_3	8.6	18
RGO/TiO_2		TBOT	hydrothermal[g]	9	80 mW cm^{-2}	Na_2S + Na_2SO_3	4.0	21
NGR/TiO_2	2.0	TBOT	solvothermal	8	150 W Xe lamp	TEOA	13.3	

[a]GC denotes graphene content in the composite. [b]TP denotes Ti precursor. [c]PM denotes preparation method. [d]PS denotes particles size. [e]SR denotes sacrificial reagent. [f]R denotes H_2 production rate of the composite. [g]Glucose as the reducing agent.

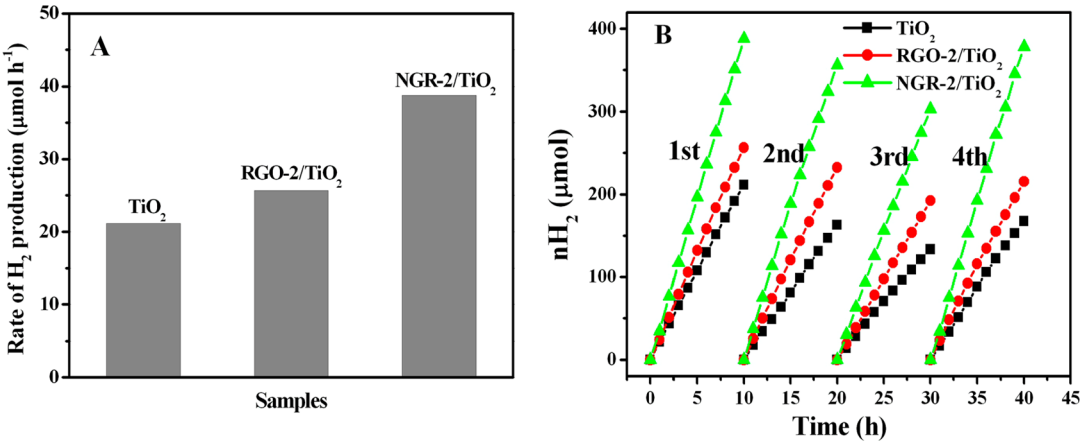

Figure 8. (A) Comparison of the rate of hydrogen evolution in 10 h irradiation and (B) repeated runs of hydrogen production for TiO_2, RGO-2/TiO_2, and NGR-2/TiO_2 using 10 vol % TEOA aqueous solution as a sacrificial reagent and 1.0 wt % Pt as a cocatalyst. Photocatalysts concentration: 0.4 mg mL^{-1}; pH 10.8; a 150 W Xe-lamp was used as the light source. For the experiment of repeated runs, before the first three runs, the system was deaerated by bubbling argon into the solution for 30 min, and the catalyst was reused in the next run. For the fourth run, the photocatalysts were separated by centrifugation and reused by adding fresh TEOA solution into the catalytic systems.

completely reduced. As to NGR, N-doping can minimize the defect sites accompanied by the effective reduction of GO,[34] resulting in a high electrical conductivity. In addition, the strong coupling between TiO_2 and NGR enhances the interfacial contact of the two moieties. Therefore, NGR in the nanocomposite is more in favor of charge transfer and separation. All of these factors lead to a higher photocatalytic activity of NGR/TiO_2 for hydrogen generation from water.

Many studies have shown that loading Pt on graphene-based photocatalysts can increase photocatalytic activity.[65,70] Loading Pt of NGR/TiO_2, RGO/TiO_2, and TiO_2 enhances the hydrogen generation efficiency obviously (Figure 8A). NGR-2/TiO_2 loaded ca. 1 wt % Pt exhibits the higher rate of hydrogen evolution (38.8 μmol h^{-1}) as compared to platinized RGO-2/TiO_2 (25.7 μmol h^{-1}) and TiO_2 (21.1 μmol h^{-1}) in 10 h irradiation; the corresponding AQY for platinized NGR-2/TiO_2 was 9.6% at 365 nm.

The photocatalytic stability of platinized NGR-2/TiO_2, RGO-2/TiO_2, and TiO_2 (1 wt % Pt) catalysts is demonstrated in Figure 8B. Before the first three runs, the system was deaerated by bubbling argon into the solution for 30 min, and the catalyst was reused in the next run. For the fourth run, the photocatalysts were separated by centrifugation and reused by adding fresh TEOA solution into the catalytic systems. To all catalysts, the amount of hydrogen evolution decreased in the second and third runs. This is partly due to the depletion of TEOA during the reaction,[71] as proved by the partial revival of photocatalytic activity when fresh TEOA solution was added in the fourth run. The stability of the catalysts was estimated by comparing the amount of hydrogen evolved from run 4 and run 1. NGR-2/TiO_2 shows a very stable photostability, and 97% hygrogen generation was recovered in the fourth run, while the value was 84% for RGO-2/TiO_2 and 79% for TiO_2. The rates of hydrogen evolution for platinized NGR-2/TiO_2, RGO-2/TiO_2, and TiO_2 were 37.8, 21.5, and 16.7 μmol h^{-1} in the fourth run, respectively. The decrease of activity is known due to the agglomeration and the loss of Pt nanoparticles on the catalysts' surface.[72] The theoretical study has shown that loading Pt on NGR sheets can increase the binding energy of Pt atoms to the substrate.[73] The nice stability of platinized NGR-2/TiO_2 indicates Pt nanoparticles can anchor on NGR surface firmly; thus the migration and loss of the Pt nanoparticles from the catalyst may be prevented.

4. CONCLUSIONS

In summary, we have successfully prepared TiO_2 nanoparticles-functionalized N-doped graphene nanocomposites (NGR)/TiO_2 via solvothermal method. The strong coupling between TiO_2 and NGR enhances the interfacial contact of the two moieties, which in turn improves the efficiency of the photoinduced charge transfer and separation. The platinized NGR/TiO_2 nanocomposite used as the photocatalyst for hydrogen generation from water demonstrates excellent activity and durability. Our study not only confirms that NGR is a superior supporting matrix to incorporate semiconductors and noble metals cocatalysts for efficient photocatalytic hydrogen generation, but also provides a promising strategy toward facile production of N-doped graphene-based nanocomposites with necessary interfacial interactions among the moieties of the composite.

■ ASSOCIATED CONTENT

Supporting Information

XRD patterns of pure TiO_2 and NGR-x/TiO_2 in Figure S1, UV−vis diffuse reflectance spectra of pure TiO_2 and NGR-x/TiO_2 in Figure S2, and the effect of pH value of the reaction system on hydrogen evolution for NGR-2/TiO_2 in Figure S3. This material is available free of charge via the Internet at http://pubs.acs.org.

■ AUTHOR INFORMATION

Corresponding Authors

*Tel.: +86-512-6588 0361. Fax: +86-512-6588 0089. E-mail: pyang@suda.edu.cn.
*E-mail: clu@chem.utoronto.ca.

Notes

The authors declare no competing financial interest.

■ ACKNOWLEDGMENTS

We are grateful for the financial support of this research by the National Natural Science Foundation of China (21373143, 51273141, and 21373103), the Priority Academic Program Development of Jiangsu Higher Education Institutions (PAPD), the Natural Scientific Foundation for Universities in Jiangsu Province (12KJJB150008), the Application Basis Research Program of Changzhou (CJ20120022), and Grand-ChallengeCanada-Rising Star Program (GCC-CRC3 0099-01).

■ REFERENCES

(1) Bonaccorso, F.; Sun, Z.; Hasan, T.; Ferrari, A. C. Graphene Photonics and Optoelectronics. *Nat. Photonics* **2010**, *4*, 611−622.
(2) Liu, Y.; Dong, X.; Chen, P. Biological and Chemical Sensors Based on Graphene Materials. *Chem. Soc. Rev.* **2012**, *41*, 2283−2307.
(3) Machado, B. F.; Serp, P. Graphene-Based Materials for Catalysis. *Catal. Sci. Technol.* **2012**, *2*, 54−75.
(4) Xiang, Q.; Yu, J.; Jaroniec, M. Graphene-Based Semiconductor Photocatalysts. *Chem. Soc. Rev.* **2012**, *41*, 782−796.
(5) Zhang, N.; Zhang, Y.; Xu, Y. J. Recent Progress on Graphene-Based Photocatalysts: Current Status and Future Perspectives. *Nanoscale* **2012**, *4*, 5792−5813.
(6) Kamat, P. V. Graphene-Based Nanoassemblies for Energy Conversion. *J. Phys. Chem. Lett.* **2011**, *2*, 242−251.
(7) Pumera, M. Graphene-Based Nanomaterials for Energy Storage. *Energy Environ. Sci.* **2011**, *4*, 668−674.
(8) Zhan, D.; Yan, J.; Lai, L.; Ni, Z.; Liu, L.; Shen, Z. Engineering the Electronic Structure of Graphene. *Adv. Mater.* **2012**, *24*, 4055−4069.
(9) Geim, A. K.; Novoselov, K. S. The Rise of Graphene. *Nat. Mater.* **2007**, *6*, 183−191.
(10) Xiang, Q.; Yu, J.; Jaroniec, M. Preparation and Enhanced Visible-Light Photocatalytic H_2-Production Activity of Graphene/C_3N_4 Composites. *J. Phys. Chem. C* **2011**, *115*, 7355−7363.
(11) Xiang, Q.; Yu, J.; Jaroniec, M. Synergetic Effect of MoS_2 and Graphene as Cocatalysts for Enhanced Photocatalytic H_2 Production Activity of TiO_2 Nanoparticles. *J. Am. Chem. Soc.* **2012**, *134*, 6575−6578.
(12) Wang, P.; Wang, J.; Ming, T.; Wang, X.; Yu, H.; Yu, J.; Wang, Y.; Lei, M. Dye-Sensitization-Induced Visible-Light Reduction of Graphene Oxide for the Enhanced TiO_2 Photocatalytic Performance. *ACS Appl. Mater. Interfaces* **2013**, *5*, 2924−2929.
(13) Yang, M. Q.; Xu, Y. J. Selective Photoredox Using Graphene-Based Composite Photocatalysts. *Phys. Chem. Chem. Phys.* **2013**, *15*, 19102−19118.
(14) Zhang, N.; Yang, M. Q.; Tang, Z. R.; Xu, Y. J. CdS-Graphene Nanocomposites as Visible Light Photocatalyst for Redox Reactions in Water: A Green Route for Selective Transformation and Environmental Remediation. *J. Catal.* **2013**, *303*, 60−69.
(15) Zhang, N.; Zhang, Y.; Yang, M. Q.; Tang, Z. R.; Xu, Y. J. A Critical and Benchmark Comparison on Graphene-, Carbon Nanotube-, and Fullerene-Semiconductor Nanocomposites as Visible Light Photocatalysts for Selective Oxidation. *J. Catal.* **2013**, *299*, 210−221.
(16) Chen, X.; Mao, S. S. Titanium Dioxide Nanomaterials: Synthesis, Properties, Modifications, and Applications. *Chem. Rev.* **2007**, *107*, 2891−2959.
(17) Xiang, Q.; Yu, J.; Jaroniec, M. Enhanced Photocatalytic H_2-Production Activity of Graphene-Modified Titania Nanosheets. *Nanoscale* **2011**, *3*, 3670−3678.
(18) Zhang, X. Y.; Li, H. P.; Cui, X. L.; Lin, Y. Graphene/TiO_2 Nanocomposites: Synthesis, Characterization and Application in Hydrogen Evolution from Water Photocatalytic Splitting. *J. Mater. Chem.* **2010**, *20*, 2801−2806.
(19) Tan, L. L.; Chai, S. P.; Mohamed, A. R. Synthesis and Applications of Graphene-Based TiO_2 Photocatalysts. *ChemSusChem* **2012**, *5*, 1868−1882.
(20) Zhang, X.; Sun, Y.; Cui, X.; Jiang, Z. A Green and Facile Synthesis of TiO_2/Graphene Nanocomposites and Their Photocatalytic Activity for Hydrogen Evolution. *Int. J. Hydrogen Energy* **2012**, *37*, 811−815.
(21) Shen, J.; Yan, B.; Shi, M.; Ma, H.; Li, N.; Ye, M. One Step Hydrothermal Synthesis of TiO_2-Reduced Graphene Oxide Sheets. *J. Mater. Chem.* **2011**, *21*, 3415−3421.
(22) Zhang, Y.; Tang, Z. R.; Fu, X.; Xu, Y. J. Engineering the Unique 2D Mat of Graphene to Achieve Graphene-TiO_2 Nanocomposite for Photocatalytic Selective Transformation: What Advantage does Graphene Have over Its Forebear Carbon Nanotube? *ACS Nano* **2011**, *5*, 7426−7435.
(23) Liang, Y. T.; Vijayan, B. K.; Gray, K. A.; Hersam, M. C. Minimizing Graphene Defects Enhances Titania Nanocomposite-Based Photocatalytic Reduction of CO_2 for Improved Solar Fuel Production. *Nano Lett.* **2011**, *11*, 2865−2870.
(24) Zhang, Y.; Zhang, N.; Tang, Z. R.; Xu, Y. J. Improving the Photocatalytic Performance of Graphene-TiO_2 Nanocomposites via a Combined Atratege of Decreasing Defects of Graphene and Increasing Interfacial Contact. *Phys. Chem. Chem. Phys.* **2012**, *14*, 9167−9175.
(25) Deifallah, M.; McMillan, P. F.; Cora, F. Electronic and Structural Properties of Two-Dimensional Carbon Nitride Graphenes. *J. Phys. Chem. C* **2008**, *112*, 5447−5453.
(26) Li, Y.; Zhou, Z.; Shen, P.; Chen, Z. Spin Gapless Semiconductor-Metal-Half-Metal Properties in Nitrogen-Doped Zigzag Graphene Nanoribbons. *ACS Nano* **2009**, *3*, 1952−1958.
(27) Imran Jafri, R.; Rajalakshmi, N.; Ramaprabhu, S. Nitrogen Doped Graphene Nanoplatelets as Catalyst Support for Oxygen Reduction Reaction in Proton Exchange Membrane Fuel Cell. *J. Mater. Chem.* **2010**, *20*, 7114−7117.
(28) Qu, L.; Liu, Y.; Baek, J. B.; Dai, L. Nitrogen-Doped Graphene as Efficient Metal-Free Electrocatalyst for Oxygen Reduction in Fuel Cells. *ACS Nano* **2010**, *4*, 1321−1326.
(29) Li, N.; Wang, Z.; Zhao, K.; Shi, Z.; Gu, Z.; Xu, S. Large Scale Synthesis of N-Doped Multi-Layered Graphene Sheets by Simple Arc-Discharge Method. *Carbon* **2010**, *48*, 255−259.
(30) Wei, D.; Liu, Y.; Wang, Y.; Zhang, H.; Huang, L.; Yu, G. Synthesis of N-Doped Graphene by Chemical Vapor Deposition and Its Electrical Properties. *Nano Lett.* **2009**, *9*, 1752−1758.
(31) Lin, Y. C.; Lin, C. Y.; Chiu, P. W. Controllable Graphene N-Doping with Ammonia Plasma. *Appl. Phys. Lett.* **2010**, *96*, 133110.
(32) Deng, D.; Pan, X.; Yu, L.; Cui, Y.; Jiang, Y.; Qi, J.; Li, W. X.; Fu, Q.; Ma, X.; Xue, Q.; Sun, G.; Bao, X. Toward N-Doped Graphene via Solvothermal Synthesis. *Chem. Mater.* **2011**, *23*, 1188−1193.
(33) Li, X.; Wang, H.; Robinson, J. T.; Sanchez, H.; Diankov, G.; Dai, H. Simultaneous Nitrogen Doping and Reduction of Graphene Oxide. *J. Am. Chem. Soc.* **2009**, *131*, 15939−15944.
(34) Mou, Z.; Chen, X.; Du, Y.; Wang, X.; Yang, P.; Wang, S. Forming Mechanism of Nitrogen Doped Graphene Prepared by Thermal Solid-State Reaction of Graphite Oxide and Urea. *Appl. Surf. Sci.* **2011**, *258*, 1704−1710.

(35) Moon, I. K.; Lee, J.; Ruoff, R. S.; Lee, H. Reduced Graphene Oxide by Chemical Graphitization. *Nat. Commun.* **2010**, *1*, 1−6.
(36) Jia, L.; Wang, D. H.; Huang, Y. X.; Xu, A. W.; Yu, H. Q. Highly Durable N-Doped Graphene/CdS Nanocomposites with Enhanced Photocatalytic Hydrogen Evolution from Water under Visible Light Irradiation. *J. Phys. Chem. C* **2011**, *115*, 11466−11473.
(37) Zhang, H.; Zhu, Y. Significant Visible Photoactivity and Antiphotocorrosion Performance of CdS Photocatalysts after Monolayer Polyaniline Hybridization. *J. Phys. Chem. C* **2010**, *114*, 5822−5826.
(38) Pei, F.; Xu, S.; Zuo, W.; Zhang, Z.; Liu, Y.; Cao, S. Effective Improvement of Photocatalytic Hydrogen Evolution via a Facile in-Situ Solvothermal N-Doping Strategy in N-TiO_2/N-graphene Nanocomposite. *Int. J. Hydrogen Energy* **2014**, *39*, 6845−6852.
(39) Meng, F.; Li, J.; Cushing, S. K.; Zhi, M.; Wu, N. Solar Hydrogen Generation by Nanoscale *p-n* Junction of *p*-type Molybdenum Disulfide/*n*-type Nitrogen-Doped Reduced Graphene Oxide. *J. Am. Chem. Soc.* **2013**, *135*, 10286−10289.
(40) Chen, P.; Xiao, T. Y.; Li, H. H.; Yang, J. J.; Wang, Z.; Yao, H. B.; Yu, S. H. Nitrogen-Doped Graphene/ZnSe Nanocomposites: Hydrothermal Synthesis and Their Enhanced Electrochemical and Photocatalytic Activities. *ACS Nano* **2012**, *6*, 712−719.
(41) Hummers, W. S.; Offeman, R. E. Preparation of Graphitic Oxide. *J. Am. Chem. Soc.* **1958**, *80*, 1339.
(42) Zhong, J.; Deng, J. J.; Mao, B. H.; Xie, T.; Sun, X. H.; Mou, Z. G.; Hong, C. H.; Yang, P.; Wang, S. D. Probing Solid State N-Doping in Graphene by X-ray Absorption Near-Edge Structure Spectroscopy. *Carbon* **2012**, *50*, 335−338.
(43) Pan, X.; Zhao, Y.; Liu, S.; Korzeniewski, C. L.; Wang, S.; Fan, Z. Comparing Graphene-TiO_2 Nanowire and Graphene-TiO_2 Nanoparticle Composite Photocatalysts. *ACS Appl. Mater. Interfaces* **2012**, *4*, 3944−3950.
(44) Kraeutler, B.; Bard, A. J. Heterogeneous Photocatalytic Preparation of Supported Catalysts. Photodeposition of Platinum on Titanium Dioxide Powder and Other Substrates. *J. Am. Chem. Soc.* **1978**, *100*, 4317−4318.
(45) Lee, W. J.; Lee, J. M.; Kochuveedu, S. T.; Han, T. H.; Jeong, H. Y.; Park, M.; Yun, J. M.; Kwon, J.; No, K.; Kim, D. H.; Kim, S. O. Biomineralized N-Doped CNT/TiO_2 Core/Shell Nanowires for Visible Light Photocatalysis. *ACS Nano* **2012**, *6*, 935−943.
(46) Liang, Y.; Li, Y.; Wang, H.; Zhou, J.; Wang, J.; Regier, T.; Dai, H. Co_3O_4 Nanocrystals on Graphene as a Synergistic Catalyst for Oxygen Reduction Reaction. *Nat. Mater.* **2011**, *10*, 780−786.
(47) Sathish, M.; Viswanathan, B.; Viswanath, R. P.; Gopinath, C. S. Synthesis, Characterization, Electronic Structure, and Photocatalytic Activity of Nitrogen-Doped TiO_2 Nanocatalyst. *Chem. Mater.* **2005**, *17*, 6349−6353.
(48) Huang, Q.; Tian, S.; Zeng, D.; Wang, X.; Song, W.; Li, Y.; Xiao, W.; Xie, C. Enhanced Photocatalytic Activity of Chemically Bonded TiO_2/Graphene Composites Based on the Effective Interfacial Charge Transfer through the C-Ti Bond. *ACS Catal.* **2013**, *3*, 1477−1485.
(49) Chen, X.; Burda, C. Photoelectron Spectroscopic Investigation of Nitrogen-Doped Titania Nanoparticles. *J. Phys. Chem. B* **2004**, *108*, 15446−15449.
(50) Mou, Z.; Han, M.; Li, G.; Du, Y.; Yang, P.; Zhang, H.; Deng, Z. Pt Nanoparticles Modified by Rare Earth Oxides: Electronic Effect and Influence to Catalytic Hydrogenation of 3-Phenoxybenzaldehyde. *Mater. Res. Bull.* **2013**, *48*, 4780−4784.
(51) Zhang, W. F.; He, Y. L.; Zhang, M. S.; Yin, Z.; Chen, Q. Raman Scattering Study on Anatase TiO_2 Nanocrystals. *J. Phys. D: Appl. Phys.* **2000**, *33*, 912−916.
(52) Bassi, A. L.; Cattaneo, D.; Russo, V.; Bottani, C. E.; Barborini, E.; Mazza, T.; Piseri, P.; Milani, P.; Ernst, F. O.; Wegner, K.; Pratsinis, S. E. Raman Spectroscopy Characterization of Titania Nanoparticles Produced by Flame Pyrolysis: The Influence of Size and Stoichiometry. *J. Appl. Phys.* **2005**, *98*, 074305−074309.
(53) Zhang, L. W.; Fu, H. B.; Zhu, Y. F. Efficient TiO_2 Photocatalysts from Surface Hybridization of TiO_2 Particles with Graphite-like Carbon. *Adv. Funct. Mater.* **2008**, *18*, 2180−2189.
(54) Zhou, W.; Pan, K.; Qu, Y.; Sun, F.; Tian, C.; Ren, Z.; Tian, G.; Fu, H. Photodegradation of Organic Contamination in Wastewaters by Bonding TiO_2/Single-Walled Carbon Nanotube Composites with Enhanced Photocatalytic Activity. *Chemosphere* **2010**, *81*, 555−561.
(55) Zhang, N.; Zhang, Y.; Pan, X.; Yang, M. Q.; Xu, Y. J. Constructing Ternary CdS-Graphene-TiO_2 Hybrids on the Flatland of Graphene Oxide with Enhanced Visible-Light Photoactivity for Selective Transformation. *J. Phys. Chem. C* **2012**, *116*, 18023−18031.
(56) Chen, Y. L.; Hu, Z. A.; Chang, Y. Q.; Wang, H. W.; Zhang, Z. Y.; Yang, Y. Y.; Wu, H. Y. Zinc Oxide/Reduced Graphene Oxide Composites and Electrochemical Capacitance Enhanced by Homogeneous Incorporation of Reduced Graphene Oxide Sheets in Zinc Oxide Matrix. *J. Phys. Chem. C* **2011**, *115*, 2563−2571.
(57) Mou, Z.; Yin, S.; Zhu, M.; Du, Y.; Wang, X.; Yang, P.; Zheng, J.; Lu, C. RuO_2/$TiSi_2$/Graphene Composite for Enhanced Photocatalytic Hydrogen Generation under Visible Light Irradiation. *Phys. Chem. Chem. Phys.* **2013**, *15*, 2793−2799.
(58) Wang, P.; Wang, Z.; Jia, L.; Xiao, Z. Origin of the Catalytic Activity of Graphite Nitride for the Electrochemical Reduction of Oxygen: Geometric Factors vs. Electronic Factors. *Phys. Chem. Chem. Phys.* **2009**, *11*, 2730−2740.
(59) Jiang, Z.; Tang, Y.; Tay, Q.; Zhang, Y.; Malyi, O. I.; Wang, D.; Deng, J.; Lai, Y.; Zhou, H.; Chen, X.; Dong, Z.; Chen, Z. Understanding the Role of Nanostructures for Efficient Hydrogen Generation on Immobilized Photocatalysts. *Adv. Energy Mater.* **2013**, *3*, 1368−1380.
(60) Zhang, N.; Zhang, Y.; Pan, X.; Fu, X.; Liu, S.; Xu, Y. J. Assembly of CdS Nanoparticles on the Two-Dimensional Graphene Scaffold as Visible-Light-Driven Photocatalyst for Selective Organic Transformation under Ambient Conditions. *J. Phys. Chem. C* **2011**, *115*, 23501−23511.
(61) Sreethawong, T.; Puangpetch, T.; Chavadej, S.; Yoshikawa, S. Quantifying Influence of Operational Parameters on Photocatalytic H_2 Evolution over Pt-Loaded Nanocrystalline Mesoporous TiO_2 Prepared by Single-Step Sol-Gel Process with Surfactant Template. *J. Power Sources* **2007**, *165*, 861−869.
(62) Jin, Z.; Zhang, X.; Li, Y.; Li, S.; Lu, G. 5.1% Apparent Quantum Efficiency for Stable Hydrogen Generation over Eosin-Sensitized CuO/TiO_2 Photocatalyst under Visible Light Irradiation. *Catal. Commun.* **2007**, *8*, 1267−1273.
(63) Zhang, X.; Jin, Z.; Li, Y.; Li, S.; Lu, G. Efficient Photocatalytic Hydrogen Evolution from Water without an Electron Mediator over Pt-Rose Bengal Catalysts. *J. Phys. Chem. C* **2009**, *113*, 2630−2635.
(64) Cheng, P.; Yang, Z.; Wang, H.; Cheng, W.; Chen, M.; Shangguan, W.; Ding, G. TiO_2-Graphene Nanocomposites for Photocatalytic Hydrogen Production from Splitting Water. *Int. J. Hydrogen Energy* **2012**, *37*, 2224−2230.
(65) Lv, X. J.; Fu, W. F.; Chang, H. X.; Zhang, H.; Cheng, J. S.; Zhang, G. J.; Song, Y.; Hu, C. Y.; Li, J. H. Hydrogen Evolution from Water Using Semiconductor Nanoparticle/Graphene Composite Photocatalysts without Noble Metals. *J. Mater. Chem.* **2011**, *22*, 1539−1546.
(66) Zhang, N.; Yang, M. Q.; Tang, Z. R.; Xu, Y. J. Toward Improving the Graphene-Semiconductor Composite Photoactivity via the Addition of Metal Ions as Generic Interfacial Mediator. *ACS Nano* **2014**, *8*, 623−633.
(67) Zhu, M.; Chen, P.; Liu, M. Graphene Oxide Enwrapped Ag/AgX (X = Br, Cl) Nanocomposite as a Highly Efficient Visible-Light Plasmonic Photocatalyst. *ACS Nano* **2011**, *5*, 4529−4536.
(68) Zhu, M.; Chen, P.; Liu, M. Ag/AgBr/Graphene Oxide Nanocomposite Synthesized via Oil/Water and Water/Oil Microemulsions: A Comparison of Sunlight Energized Plasmonic Photocatalytic Activity. *Langmuir* **2012**, *28*, 3385−3390.
(69) López, V.; Sundaram, R. S.; Gómez-Navarro, C.; Olea, D.; Burghard, M.; Gómez-Herrero, J.; Zamora, F.; Kern, K. Chemical Vapor Deposition Repair of Graphene Oxide: A Route to Highly Conductive Graphene Monolayers. *Adv. Mater.* **2009**, *21*, 4683−4686.
(70) Park, Y.; Kang, S. H.; Choi, W. Exfoliated and Reorganized Graphite Oxide on Titania Nanoparticles as an Auxiliary Co-catalyst

for Photocatalytic Solar Conversion. *Phys. Chem. Chem. Phys.* **2011**, *13*, 9425−9431.
(71) Chatterjee, D. Effect of Excited State Redox Properties of Dye Sensitizers on Hydrogen Production through Photo-Splitting of Water over TiO_2 Photocatalyst. *Catal. Commun.* **2010**, *11*, 336−339.
(72) Bai, Y.; Li, W.; Liu, C.; Yang, Z.; Feng, X.; Lu, X.; Chan, K. Y. Stability of Pt Nanoparticles and Enhanced Photocatalytic Performance in Mesoporous Pt-(Anatase/TiO_2(B)) Nanoarchitecture. *J. Mater. Chem.* **2009**, *19*, 7055−7061.
(73) Groves, M. N.; Chan, A. S. W.; Malardier-Jugroot, C.; Jugroot, M. Improving Platinum Catalyst Binding Energy to Graphene through Nitrogen Doping. *Chem. Phys. Lett.* **2009**, *481*, 214−219.